ADVANCED QUANTUM TECHNOLOGIES
www.advquantumtech.com

Single Photon Emitters Coupled to Plasmonic Waveguides: A Review

*Shailesh Kumar and Sergey I. Bozhevolnyi**

During the last two decades, many research groups have demonstrated coupling of single photon emitters to plasmonic waveguides, promising very high emission enhancements, for applications in quantum technologies. In this review, recent developments within this important research topic are discussed. Different plasmonic waveguide–quantum emitter configurations are compared from the application viewpoint by utilizing a figure-of-merit (FOM) reflecting the emission enhancement, coupling efficiency, and radiation loss. The experimental methods applied to obtain the coupled systems with high FOMs are described. Configurations that are exploited for reinforcing the coupling efficiency, i.e., the efficiency of funneling the emitted radiation into a plasmonic waveguide, are also considered as well as the scalability potential of various waveguide platforms. A recent experiment, in which enhanced light–matter interaction in a plasmonic waveguide is taken advantage of, resulting in the demonstration of non-linearity at the single emitter level, is discussed.

1. Introduction

Single photon emitters (SPEs) are crucial for photon based quantum technologies.[1–4] In last few decades, a lot of research has been done to find a good single photon emitter. Atoms and ions emit single photons, but need to be trapped and require elaborate set-up for their use in quantum optical experiments.[5] Therefore, solid-state emitters with atom like emission properties are considered to be promising for integrated quantum optics.[6–12] Solid-state emitters also have issues such as their emission in all directions, and low emission rate which make it challenging for their use in quantum technologies. Emission properties of an emitter can be modified by engineering the environment of an emitter. Two kinds of materials have been utilized for engineering the environment of the emitter—1) dielectric and 2) metallic. For both kinds of materials either waveguides or cavity can be utilized for enhancing emission properties. High index dielectric material have been utilized for fabrication of waveguides and cavities to change the environment of single photon emitters, and obtain enhanced emission properties.[13–15] However, due to the diffraction limit in dielectric structures, the enhancements in decay-rate are also limited. Plasmonic waveguides and cavities offer a bigger advantage in terms of decay-rate enhancements.[16,17] Plasmonic cavities have been utilized to obtain very high decay-rate enhancements, and plasmonic structures work for enhancement of a broad spectrum, as the cavity finesse is low.[18–21] These, however, have not been utilized, so far, for emission into waveguide structures, and therefore have not been utilized for integrated quantum technologies.[22] Plasmonic waveguides on the other hand can enhance the decay-rate as well as channel the emission into the waveguide.[23,24] The fraction of emission channeled into the waveguide is called as β-factor, which can be high for plasmonic waveguides. This offers a possibility for their utilization in integrated quantum technology.[25–32] Plasmonic waveguides, however, are lossy. Losses, β-factor and decay-rate enhancement depend a lot on the structure of the waveguide. Generally, one would like to maximize both beta-factor and decay-rate enhancement and minimize propagation loss. In this regard, one can conveniently utilize a figure-of-merit (FOM) to compare different plasmonic waveguide-quantum emitter coupled systems. The FOM is defined as the product of decay-rate enhancement, β-factor and propagation length normalized by the emission wavelength in vacuum.

In this review, first, we briefly describe a numerical method to estimate the decay-rate enhancement and β-factor. We then discuss the FOMs for various plasmonic waveguide-quantum emitter system. Subsequently, we describe some of the coupled systems with high FOMs, experimental methods used for obtaining the coupled systems and their potential for scalability. After discussing the coupled systems, we present some structures that have been used to complement the efficient channeling into a plasmonic waveguide, such as gratings and cavities. We also discuss non-linearity observed at single emitter level in a quantum emitter–plasmonic waveguide coupled system. We end this review with a conclusion.

S. Kumar, S. I. Bozhevolnyi
Centre for Nano Optics
University of Southern Denmark
Campusvej 55, Odense M, DK-5230, Denmark
E-mail: seib@mci.sdu.dk
S. I. Bozhevolnyi
Danish Institute for Advanced Study
University of Southern Denmark
Campusvej 55, Odense M, DK-5230, Denmark

The ORCID identification number(s) for the author(s) of this article can be found under https://doi.org/10.1002/qute.202100057

DOI: 10.1002/qute.202100057

2. Theory of Excitation of a Plasmonic Waveguide Mode by a Dipole Emitter

The waveguide properties, such as its mode-confinement, determine the emission rate of a quantum emitter into its modes. Total decay-rate of an emitter depends not only on the magnitude of its dipole moment, but also its position and orientation in the cross-section of the waveguide. In this section, first, a procedure to estimate waveguide modes supported by plasmonic waveguide structures is discussed. Subsequently, a numerical method to calculate decay-rate into waveguide, total decay-rate and β-factor is described. The method presented below is described in detail in ref. [24].

2.1. Plasmonic Waveguide Modes

Plasmonic waveguides can support modes confined beyond diffraction limit, because of metal permittivity having negative real part.[33] One can solve the wave equation given below, with boundary conditions suitable for the structure, and obtain modes supported by the structure:

$$\vec{\nabla} \times \frac{1}{\mu(\vec{r})}\left(\vec{\nabla} \times \vec{E}(\vec{r})\right) - k_0^2 \epsilon(\vec{r})\vec{E}(\vec{r}) = 0 \tag{1}$$

with the position $\vec{r} \equiv (x, y, z)$, the vacuum wavenumber $k_0 = \omega\sqrt{\epsilon_0 \mu_0}$, with ω being the angular frequency. ϵ_0 and μ_0 are permittivity and permeability of vacuum, respectively. $\epsilon(\vec{r})$ and $\mu(\vec{r})$ are relative dielectric function and relative permeability constant, respectively. The solution to the wave equation is given by

$$\vec{E}(x, y, z) = \vec{E}_\alpha(x, y)e^{-i(\omega t - kz)} \tag{2}$$

when the waveguide is infinitely long. Propagation direction in the above equation is assumed to be $+z$. Given an angular frequency, α (indicates transverse mode) and k (propagation constant) form a complete set of orthogonal modes for any waveguide. Numerical methods, for example, finite element method (FEM) can be utilized for calculating modes supported by any waveguide structure.[34]

2.2. Excitation of a Plasmonic Waveguide by a Quantum Emitter

When a quantum emitter is coupled to a plasmonic waveguide, it can decay via three channels as shown schematically in **Figure 1**. One channel is radiative channel, that is, quantum emitter emits a photon into the far-field when it decays. The second channel is generation of a plasmon when quantum emitter decays. And the third channel is when the quantum emitter decays non-radiatively. Depending on the waveguide structure, position and orientation of quantum emitter, decay-rate into different channels can change. For a quantum emitter coupled to a plasmonic waveguide, decay into the plasmonic waveguide mode is preferred for its application in integrated quantum technologies. The fraction of total decay-rate that excites plasmons in plasmonic waveguide is defined as

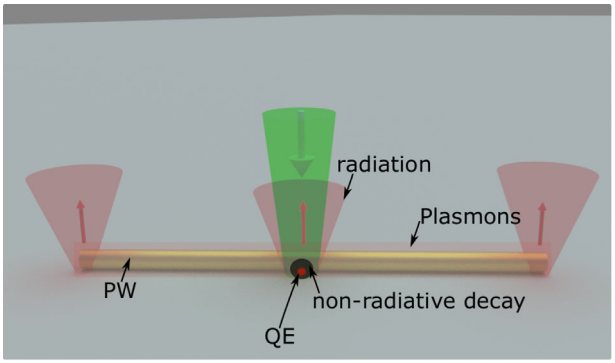

Figure 1. A schematic showing a quantum emitter coupled to a plasmonic waveguide. QE, quantum emitter; PW, plasmonic waveguide.

β-factor. In this section, we describe a procedure to calculate decay-rate into plasmon waveguide mode, total decay-rate and β-factor. With all these parameters known, one can calculate the FOM.

2.2.1. Channeling of Emission from a Dipole Emitter into a Plasmonic Mode

The local density of states (LDOS) determines the emission rate of an emitter in a particular environment. For an emitter in the vicinity of a plasmonic waveguide, the LDOS in terms of electric and magnetic field is given as[24]

$$\rho_{pl}(\vec{r}, \omega) = \frac{6\left|\vec{E}(x, y) \cdot \bar{n}_D\right|^2}{2\pi\Re\{\int_{A_\infty}\left(\vec{E} \times \vec{H}^*\right) \cdot \bar{z}dA\}} = \frac{6\left|\vec{E}(x, y) \cdot \bar{n}_D\right|^2}{Nv_g} \tag{3}$$

with group velocity

$$v_g = \frac{\Re\{\int_{A_\infty}\left(\vec{E} \times \vec{H}^*\right) \cdot \bar{z}dA\}}{\int_{A_\infty} \epsilon_0\epsilon(x, y)\left|\vec{E}(x, y)\right|^2 dA} \tag{4}$$

and normalization factor

$$N = 2\pi \int_{A_\infty} \epsilon_0\epsilon(x, y)\left|\vec{E}(x, y)\right|^2 dA \tag{5}$$

The unit vector along $+z$ direction is $\bar{z}$, and that along the dipole moment of emitter is $\bar{n}_D$. A_∞ denotes integration over the $+z$ transverse plane. The meaning of other symbols are given in Section 2.2.1.

From Equation (3), it can be observed that v_g should be small for large LDOS, and with a confined mode and optimum dipole orientation of the emitter the LDOS can be maximized. For an emitter with dipole moment $\vec{\mu}_D$, the projected LDOS determines the decay-rate,

$$\Gamma_{pl}(\vec{r}, \omega) = \frac{\pi\omega_0}{3\hbar\epsilon_0}\left|\vec{\mu}_D\right|^2 \rho_{pl}(\vec{r}, \omega) \tag{6}$$

with the Planck's constant divided by 2π denoted as $\hbar$. Derivation of Equation (6) involves quantum mechanics, as the energy

levels of SPEs are determined by laws of quantum mechanics and they emit quanta of light. For a detailed discussion of relation between LDOS and decay-rate of a quantum emitter, and derivation of Equation (6), we refer the readers to ref. [35]. Thus, the decay-rate of an emitter into a plasmonic mode normalized to its decay-rate in vacuum is given as:

$$\frac{\Gamma_{pl}(\vec{r},\omega)}{\Gamma_0} = \frac{6\pi^2 c^3 \left|\vec{E}(x,y)\cdot\bar{n}_D\right|^2}{\omega^2 N v_g} \tag{7}$$

with

$$\Gamma_0 = \frac{\omega^3 \left|\vec{\mu}_D\right|^2}{3\pi\hbar\epsilon_0 c^3} \tag{8}$$

the emitter decay-rate in vacuum.[35] Combining Equations (4), (5), and (7), the emitter decay-rate into a plasmonic mode, normalized to its decay-rate in vacuum, is the following:[24,28]

$$\frac{\Gamma_{pl}}{\Gamma_0} = \frac{3\pi c\epsilon_0 \left|\vec{E}(x,y)\cdot\bar{n}_D\right|^2}{\Re\{k_0^2 \int_{A_\infty} \left(\vec{E}\times\vec{H}^*\right)\cdot\vec{z}dA\}} \tag{9}$$

2.2.2. Total Decay-Rate and β-Factor of an Emitter

The total decay-rate of an emitter consists of decay-rate into plasmonic mode, radiation into far-field and non-radiative decay. To calculate the total decay-rate, a three dimensional model can be utilized. One can calculate the total decay-rate by solving the following equation,[24]

$$\left[\vec{\nabla}\times\vec{\nabla}\times -k_0^2\epsilon(\vec{r})\right]\vec{E}(\vec{r},\omega) - i\omega\mu_0\vec{J}(\omega) = 0 \tag{10}$$

with the current density denoted by $\vec{J}(\omega)$.

With suitable boundary conditions in different environments, and comparing the power emitted by the emitter one can estimate the decay-rate enhancements. Power dissipated by a current source near a plasmonic waveguide is given as[24]

$$P_{\text{total}} = \frac{1}{2}\int\int\int \Re\left(\vec{J}^*\cdot\vec{E}\right)dV \tag{11}$$

Similarly, power dissipated by a current source in vacuum is given by

$$P_0 = \frac{1}{2}\int\int\int \Re\left(\vec{J}^*\cdot\vec{E}_0\right)dV \tag{12}$$

Therefore, the total decay-rate, normalized to decay-rate in vacuum, is as follows:

$$\frac{\Gamma_{\text{total}}}{\Gamma_0} = \frac{P_{\text{total}}}{P_0} \tag{13}$$

With the decay-rate into the plasmonic mode (Equation (9)) and total decay-rate (Equation (13)), the β-factor is given as follows:[23,24]

$$\beta = \frac{\Gamma_{pl}}{\Gamma_{\text{total}}} \tag{14}$$

3. Experimental Realizations of Various Coupled Systems

The maximum decay-rate enhancement, β-factor and propagation lengths depend on the waveguide structure. Furthermore, decay-rate enhancement and β-factor depends on the position of emitter as well as its orientation in the waveguide cross-section. There can be various FOMs that can be used to compare different systems. For example, beta-factor, decay-rate enhancement or the propagation lengths of the waveguide can each be an FOM, on its own, depending on the application. Here, we have chosen an FOM that is a product of all the three merits normalized by the emission wavelength, to compare various systems as this indicates overall which system is performing better. This FOM should be used with caution, because if the systems will be very different from each other, for example, in the case of plasmonic and dielectric waveguide, then one of the parameters will be dominating and it may not be a useful comparison. However, if the systems are similar, then this FOM can be utilized as is the case for plasmonic waveguide-SPE systems discussed in this review article. We note that even for plasmonic waveguide-SPE systems, depending on the application, various merits (demerits) should be compared independently to choose a particular system. To maximize the FOM, as defined earlier, the emitter should be placed at an optimum position. This is an experimental challenge towards which different research groups have tried to solve using different techniques, some of which are described in this review. In this section, we give an overview of experimental demonstrations of coupling a single photon emitter to different plasmonic waveguides.

In **Figure 2**, we compare FOMs and propagation lengths of different quantum emitter–plasmonic waveguide coupled systems reported in the literature. We observe that FOMs vary between 2 and 500 depending on the waveguide structure, material and quantum emitter.[36–43] The system with an FOM of 4.2 was the pioneering work by Akimov et al.[36] After this demonstration, many experimental studies have been performed for quantum emitters coupled with single silver nanowires.[44–52] In 2013, quantum emitters were coupled to gap-mode plasmonic waveguide in a dual wire system, and a FOM of ≈23 was demonstrated.[37] Later, V-grooves coupled to single photon emitters were demonstrated.[38,53] These systems have been reviewed by A. Huck et al.[54] Also, dibenzoterrylene (DBT) molecules were coupled to hybrid plasmonic waveguides, where a plasmonic slot structure was used together with dielectric layers in order to utilize the plasmonic structure to efficiently couple to the molecules.[55] The FOM for this structure is 2.2 as the gap in the plasmonic slot is 200 nm wide. In **Table 1**, properties of various coupled systems are presented. In the following, we present various quantum emitter–plasmonic waveguide coupled systems with FOM larger than 50, as presented above the dotted line in Figure 2. We describe the plasmonic structure, methods utilized

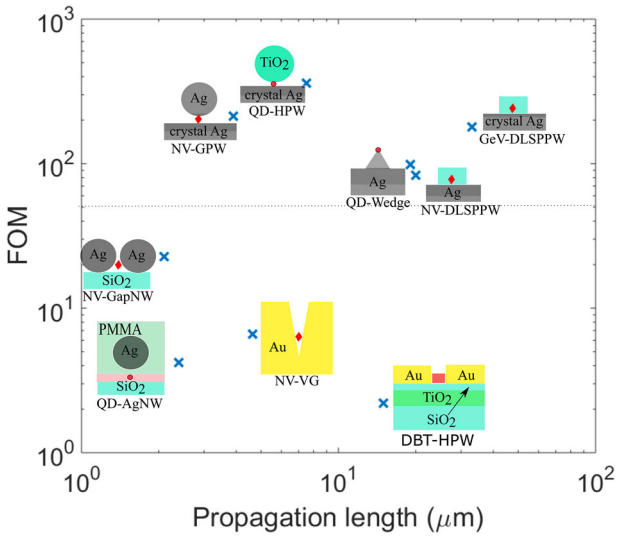

Figure 2. FOM versus propagation length of different quantum emitter-plasmonic waveguide coupled systems. QD-AgNW: quantum dots coupled to silver nanowires.[36] NV-GapNW, nitrogen vacancy (NV) centers in nanodiamonds coupled to gap plasmon mode between two parallel silver nanowires.[37] NV-VG, NV centers coupled to plasmonic V-groove waveguides.[38] QD-Wedge, quantum dots coupled to silver wedge waveguides.[39] NV-DLSPPW, NV centers coupled to dielectric loaded surface plasmon polariton waveguides.[40] GeV-DLSPPW, germanium vacancy (GeV) centers coupled to dielectric loaded surface plasmon polariton waveguides.[41] "crystal Ag" denotes monocrystalline silver flakes utilized in the experiment. NV-GPW, NV centers in nanodiamonds coupled to gap plasmon waveguide mode supported by gap between silver flakes and silver nanowires.[42] QD-HPW, quantum dots coupled to hybrid plasmonic modes.[43] DBT-HPW, dibenzoterrylene (DBT) molecules coupled to a hybrid plasmonic waveguide.[55] We note that all the experiments involving silver nanowires mentioned in this comparison utilize chemically grown monocrystalline silver nanowires.

to fabricate the coupled systems, resulting decay-rate enhancements and FOMs.

3.1. Excitation of Wedge Waveguide Modes by Colloidal Quantum Dots

As defined in Section 2.2, the FOM for a wedge waveguide mode coupled to a colloidal quantum dot can be high as demonstrated in ref. [39]. For the optimized structure, in **Figure 3**a,b, we present the electric field distribution and decay-rate into plasmonic waveguide mode normalized to its decay-rate in vacuum, respectively, following the procedure presented in Section 2.1.

To get an angle of 70.54°, 100-oriented silicon wafer was etched using an anisotropic method. Subsequently, a thick silver layer (thickness > 350 nm) was deposited. The silver was deposited at a high deposition rate (2.5 nm s^{-1}) and low residual gas pressure (3×10^{-8} Torr). According to ref. [39], the silver film thus obtained had properties like mono-crystalline silver. Template stripping was then used to obtain smooth and sharp apexes.

In this experiment, colloidal quantum dots (QDs) were utilized as quantum emitters. Colloidal QDs are promising for quantum technologolies.[56] The QDs were deposited near the apexes of wedge waveguides by using electro-hydro-dynamic (EHD) printing. Even single QD can be deposited using this technique, as can be seen in Figure 3j. In Figure 3c, a false color fluorescence image is presented where a wedge waveguide can be seen with three QDs near the apex. The image was obtained by averaging one thousand frames, each of one second. In the image, the three QDs are indicated as QD1, QD2, and QD3. Blinking pattern as seen from Figure 3d–g clearly suggests that these spots are generated by single QDs. QD2 blinking and the wedge waveguide end blinking could be correlated, as shown in Figure 3h,i. This clearly proved that the wedge waveguide was excited by QD2. Similarly, the blinking of QD1 and QD3 could not be correlated to wedge waveguide end emission. This could happen if the QD1 and QD3 were not close enough to the apex of the waveguide.

In the above experiment, by positioning of emitters at the right positions, well coupled systems could be obtained. This underlines the importance of positioning of emitters with respect to the waveguide. In this experiment, the lifetime for QDs in tetradecane and that on the apex of the wedge waveguide, was compared. 4.64 was the observed total decay-rate enhancement. With a propagation length of 19 μm, the FOM for this system is calculated to be 98. Although the FOM of this system is high, it is difficult to scale this system due to the way these waveguides were fabricated. For this way of fabrication, it will be hard to fabricate on-chip optical components such as beam-splitters and routers.

3.2. Coupling Single Emitters to Dielectric Loaded Surface Plasmon Polariton Waveguide

Dielectric loaded surface plasmon polariton (DLSPP) waveguide is one other structure that provides a balance of confinement

Table 1. Properties of coupled systems.

Coupled systems	Propagation length (μm)	FOM	β-factor	Decay-rate enhancement	Wavelength (nm)
QD-AgNW	2.4	4.2	0.6	2	655
NV-GapNW	2.1	22.7	0.91	8.3	700
NV-VG	4.65	6.6	0.42	2.3	680
QD-Wedge	19	98	0.70	4.64	630
NV-DLSPPW	20	83	0.58	5	700
GeV-DLSPPW	33	180	0.56	6	602
NV-GPW	3.9	212	0.76	49.8	700
QD-HPW	7.5	361	0.73	41.5	630
DBT-HPW	15	2.2	0.115	1	780

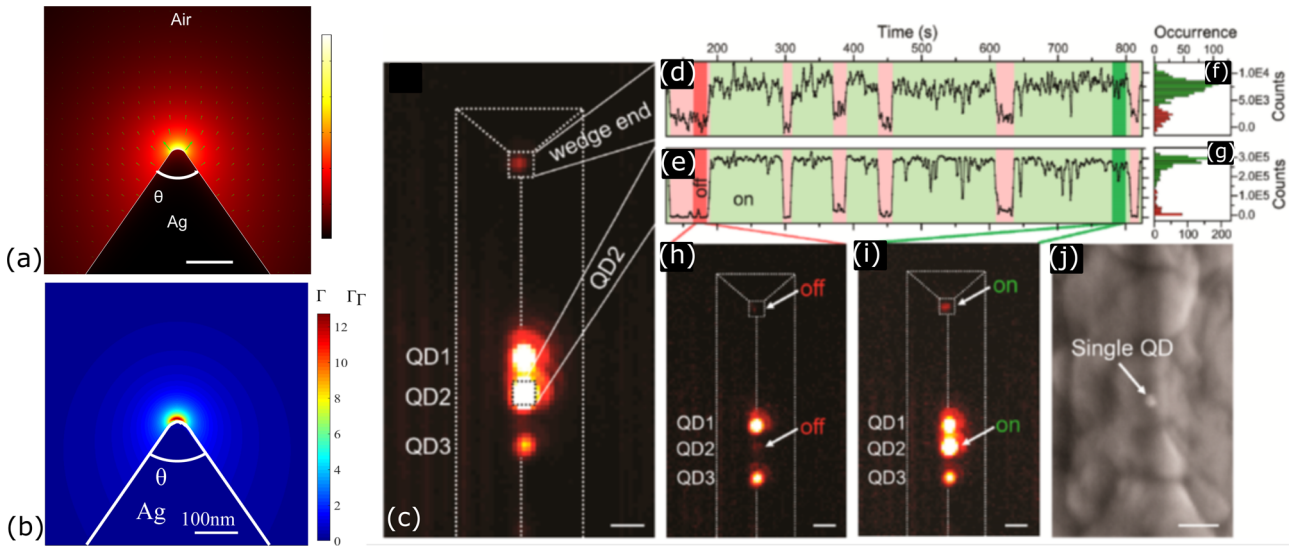

Figure 3. a) Distribution of electric field for the fundamental mode supported by wedge waveguide. b) Decay-rate of an emitter into the wedge waveguide mode, normalized to its decay-rate in vacuum. c) False-color image of a wedge waveguide apex with three different spots (QD1, QD2 and QD3) near the apex of the wedge waveguide. d,e) The fluorescence intensities extracted as a time-series from the wedge waveguide end and QD2, respectively. A strong correlation in the two signals can be observed, as they exhibit same on and off periods. f,g) Histograms for the wedge end and QD2, respectively, where a bimodal distribution in intensity can be observed. h,i) 20 frames of the off and the on state, respectively, of integrated fluorescence images as indicated. Scalebars in (c,h,i) correspond to 1 μm. j) A single QD can be seen in the scanning electron micrograph (SEM) image near the apex of the silver wedge (scale bar 40 nm). Reproduced with permission.[39] Copyright 2015, The American Chemical Society.

and propagation losses. Therefore, FOM can be high for DLSPP waveguide as has been shown in refs. [40] and [41]. Below, we briefly describe these two experiments.

In ref. [40], a nitrogen vacancy (NV) center in a nanodiamond was coupled to a DLSPP waveguide. NV centers in diamonds have many suitable properties which makes it useful for quantum information processing.[57–64] NV center is a source of stable single photon emission at room temperature. Other properties that has made NV centers useful for quantum technologies is their long spin coherence times and optical read-out of spins. For the metal surface, a silicon wafer coated with thermally deposited silver was used. In **Figure 4**a, decay-rate of the emitter into plasmonic mode Γ_{pl}/Γ_0, normalized by decay-rate in vacuum, shows up to a threefold emission enhancement at the optimum position. Inset in the figure illustrates the position of emitter inside the DLSPP waveguide cross-section. The position dependence of the decay-rate into plasmonic mode normalized to decay-rate in vacuum (Γ_{pl}/Γ_0) and β-factors are shown in Figure 4b.

For fabricating the sample, a silver film of thickness 250 nm was deposited on silicon. Gold markers were fabricated on them, and subsequently, nanodiamonds containing single NV centers were spin-coated. In a fluorescence confocal microscope, the fluorescence scan map was taken as shown in Figure 4c. Gold markers (+) and a nanodiamond can be observed in the fluorescence image. Lifetime, spectrum, and correlation measurements were taken for the NV nanodiamonds. To fabricate the waveguide with the pre-characterized NV nanodiamond embedded, hydrogen silsesquioxane (HSQ) was used. HSQ is a negative electron beam resist (Dow Corning XR-1541-006). HSQ was spin-coated (1200 rpm, 1 min) to get a 180 nm film on the silver surface. Waveguide was fabricated embedding the nanodiamond containing single NV centers using electron beam lithography. An atomic force microscope (AFM) image of such a waveguide is presented in Figure 4d. In Figure 4e, the fluorescence image, taken after fabrication of waveguide when the NV center is excited continuously, is presented. The image shows emission from the gratings at the two ends, in addition to the NV center spot. This clearly indicates the coupling of NV center to the DLSPP waveguide.

Second-order autocorrelation for NV center after fabrication of the waveguide is presented in Figure 4f. A model presented in ref. [65], is utilized to fit the data. $g^2(0) < 0.5$ clearly indicates that a single photon emitter was coupled to the waveguide. A cross-correlation between NV center and spot B is shown in Figure 4g, with $g^2(0) < 0.5$, which indicate that spots NV center and B originate from the same single NV center. Aslo a lifetime comparison of the NV-center before and after coupling is presented in Figure 4h, where a lifetime reduction from ≈10 to ≈6 ns is observed. Tail-fitting with a single exponential of the measured data was used to estimate the lifetimes. Background fluorescence has a short lifetime, therefore first few ns of the measured data was not used for fitting. Lifetime reduction in the range 1.5 to 3.1 were observed in the experiment after the fabrication of waveguide. On average, the NV center lifetime decreased by a factor of ≈2.5. Also, NV center lifetimes decreased due to a silver surface by a factor of 2, on average, when compared to lifetime of NV centers in nanodiamonds placed on a fused silica surface. Therefore, the total decay rate enhancement for this experiment was reported as $\Gamma_{tot}/\Gamma_0 = 5 \pm 1$. With $\beta = 0.58 \pm 0.03$, propagation length $L_p = 20 \pm 5$ μm and $\lambda = 700$ nm, an FOM of 83 ± 15 was obtained.

In addition to a high FOM, such waveguides were utilized for demonstrating routing of single plasmons between two waveguides. A directional coupler (DC) with two DLSPP waveguides

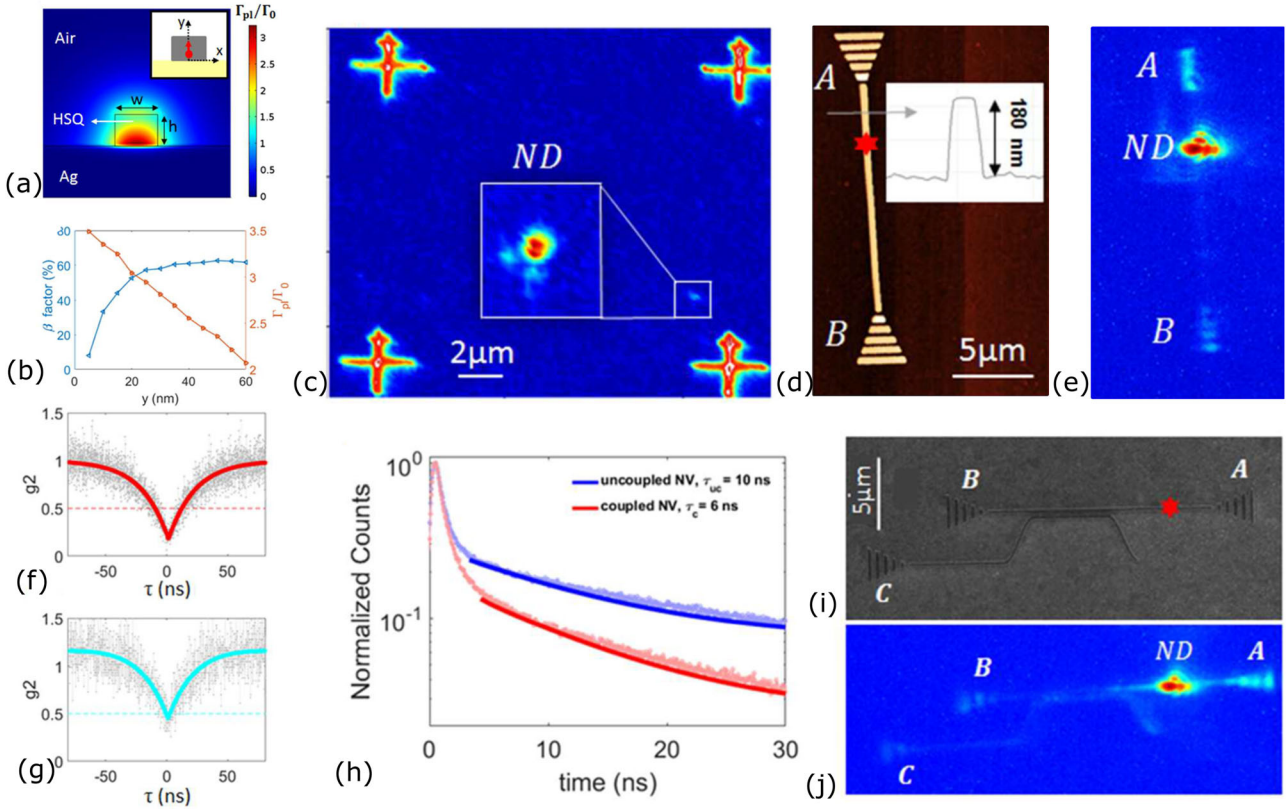

Figure 4. a) Decay-rate of an emitter in DLSPP waveguide normalized to its decay-rate in vacuum, Γ_{pl}/Γ_0. The inset indicates the position of emitter inside the DLSPP waveguide cross-section. b) Position dependence of the plasmonic decay-rate and β-factor for DLSPP waveguide for a y-oriented dipole. c) Fluorescence map of an area with gold markers and nanodiamonds spin-coated on a silver surface. d) AFM image of the fabricated waveguide. In the inset, a 180 nm height for the waveguide can be observed. e) Fluorescence image of the waveguide structure where the nanodiamond is continuously excited. Emission from the gratings at the ends of the waveguide, in addition to the NV center spot confirms the excitation of the waveguide mode. f) Autocorrelation measured and a model fit for the NV center. g) Cross-correlation between NV center and spot B after fabrication of the waveguide. τ denotes time delay. h) Lifetime comparison of the NV center before (blue) and after (red) fabrication of the waveguide. i) SEM image of a DLSPP-based directional coupler. The red spot indicates the position of the nanodiamond. j) CCD camera image of the directional coupler structure recorded with continuous excitation of the ND. Adapted with permission.[40] Copyright 2017, The American Chemical Society.

having a parallel section was fabricated. The DC coupler parameters were height $h = 180$ nm, width $w = 250$ nm, the gap between waveguides in the parallel region $g = 200$ nm. The coupling length for DC with afore-mentioned parameters was calculated to be $L_c = 5.3$ μm. This length is required for imparting a π phase between symmetric and anti-symmetric modes supported in the DC. Following the same procedure, as for DLSPP waveguides, one of the waveguides was embedded with nanodiamond containing a single NV-center. An SEM image of the fabricated DC is presented in Figure 4i. Fluorescence image of the DC in Figure 4j, while the NV center embedded in one of the waveguides is excited, shows the coupling of the NV center to the DC structure. In addition to the NV spot, there is emission from ends A, B, and C. The emission from end C clearly suggests that single plasmons were routed to the second waveguide, which did not contain the nanodiamond with single NV center.

In another experiment,[41] germanium vacancy (GeV) centers were coupled to DLSPP waveguide supported by HSQ on a monocrystalline silver flake. GeV centers in diamonds are a source of single photons at room temperature, and has also been shown to emit indistinguishable photons at cryogenic temperatures.[66,67] In addition, up to 70% of the emission at cryogenic temperatures is in their zero-phonon lines (ZPL). Therefore, they are promising candidate for photon-based quantum technologies. GeV centers in nanodiamonds utilized in this experiment were grown with a high-pressure high-temperature technique.

In this experiment, a long propagation length of green light ($\lambda = 532$ nm) of 11.8 μm and a high coupling efficiency of 12% was utilized to remotely excite a nanodiamond containing a single GeV center embedded in a DLSPP waveguide. To prepare the sample, first, a silicon sample was coated by a thermally deposited silver film. Monocrystalline silver flakes fabricated chemically were, subsequently, spin-casted on the sample. Gold markers were fabricated, like the one utilized in the afore-mentioned experiment, on silver flakes. GeV nanodiamonds were then spin-coated. For embedding single GeV nanodiamonds in DLSPP waveguide, HSQ structure was fabricated following the procedure described previously in this section. A schematic of the fabricated device is presented in **Figure 5**a. Left panel of Figure 5b shows an AFM image of the waveguide fabricated embedding the nanodiamond. A fluorescence image, when the green

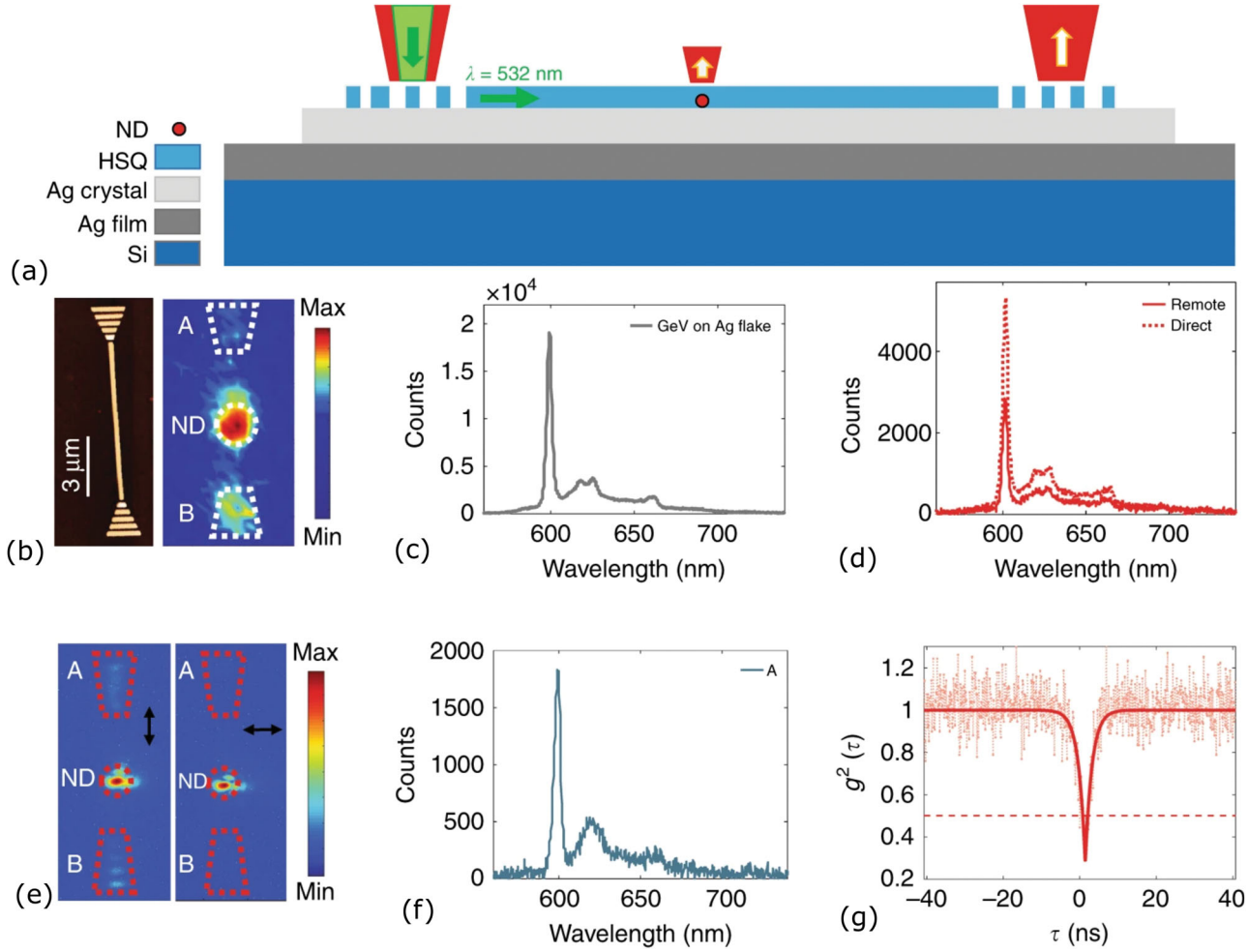

Figure 5. a) Schematic of the sample used for remotely exciting a GeV nanodiamond embedded in a DLSPP waveguide. b) AFM image of the fabricated waveguide (b, left) and a galvanometric mirror scan image, where the excitation laser is continuously illuminated at end B (b, right). c) Emission spectrum of the GeV nanodiamond before fabrication of DLSPP waveguide. d) Emission spectrum measured for the coupled GeV when excited remotely (d, solid line) and when the GeV is excited remotely (d, dotted line). e) Fluorescence images with a linear polarizer placed along (left) and perpendicular (right) to the waveguide axis in the detection path for the coupled system when GeV nanodiamond is excited directly. f) Emission spectrum taken for the outcoupled light at end A in the case of remote excitation. g) Second order correlation function of the GeV emitter confirming a single photon emission. Adapted with permission.[41] Copyright 2018, Nature Publishing Group.

excitation laser was coupled into the waveguide by shining at end B, is presented in the right panel of Figure 5b. Fluorescence emission from GeV nanodiamond embedded inside the waveguide, in addition to emission from ends A and B, confirmed a remote excitation of the GeV center. Figure 5c and d shows emission spectra of the GeV center excited before coupling to waveguide, and after coupling, which are similar in terms of their shape, as can be expected. In Figure 5e, fluorescence images with GeV center being excited directly, and with a linear polarizer placed in the detection path, as indicated in the images, are shown. By comparing the two images in Figure 5e, one can observe that the emission from waveguide ends is polarized. This results from coupling of emission to DLSPP waveguide mode, which propagates to waveguide ends and is scattered by the gratings. In Figure 5f, the spectrum measured at the end A, with the GeV center remotely excited is presented. In Figure 5g, the second-order correlation function measured for the GeV center confirms it as a single photon emitter ($g^2(0) < 0.5$). The GeV-DLSPP waveguide hybrid system with a FOM value of up to 180 ± 25, due to $\Gamma_{tot}/\Gamma_0 = 6 \pm 1$, $\beta = 0.56 \pm 0.03$, and $L_p = 33 \pm 3$ μm at a wavelength of $\lambda = 602$ nm, is indeed a promising combination of the emitter and waveguide.

From above experiments, it is clear that DLSPP waveguides coupled to color centers in nanodiamonds can have high FOM, and they can be used for routing of single plasmons. Therefore, this waveguide–quantum emitter coupled system has the potential for scalability.

3.3. Excitation of Gap-Plasmon Waveguides by Quantum Emitters

Extremely confined modes can be supported by gap-plasmon waveguides. Therefore, very high enhancement of decay-rate can

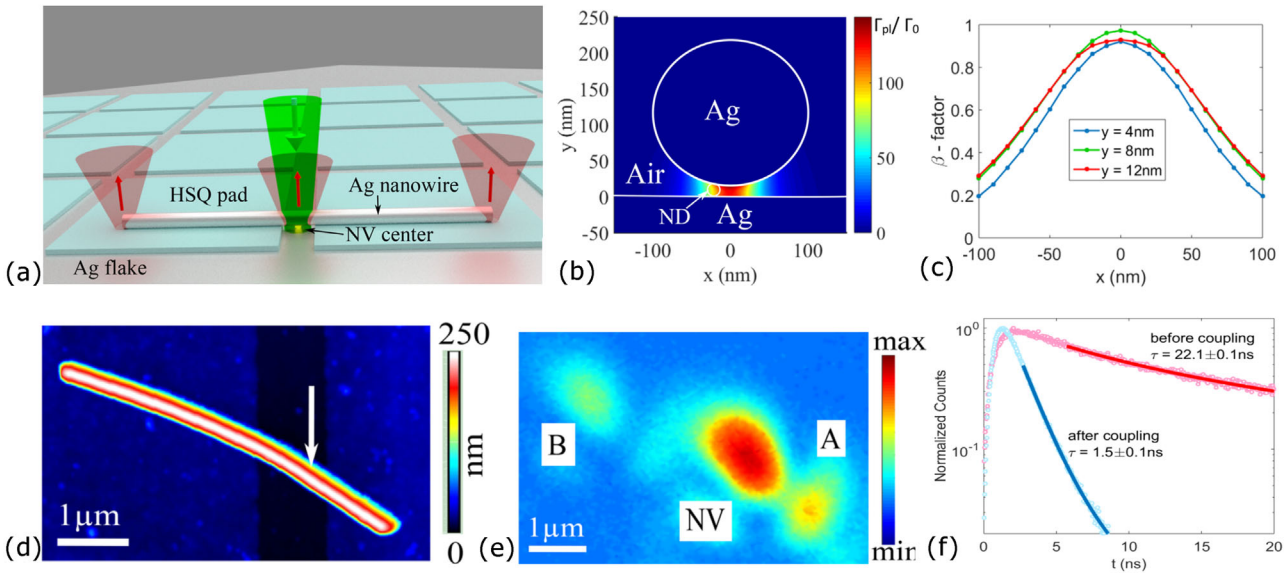

Figure 6. a) Schematic showing the silver flake with HSQ pads supporting silver nanowire. A nanodiamond excited by a green laser is also illustrated. The emission couples to gap-mode between wire and flake, propagates to the end of the nanowire and gets scattered subsequently. b) Decay-rate of emitter into the gap-plasmonic mode, normalized to its decay-rate in vacuum. Position of the nanodiamond, as estimated according to dimensions involved. ND, nanodiamond. c) β-factor vs position of emitter. d) AFM image of silver nanowire placed on top of nanodiamond, which is put in the gap between two HSQ pads on the flake, forming the coupled system. e) Fluorescence image when the NV spot is excited, emission coupled to gap-plasmon waveguide and gets scattered from silver nanowire ends (Spots A and B). f) Lifetime comparison for the NV center. Measured data (dots) and a single exponential fit (continuous line) are shown for the NV center before and after the silver nanowire is put on top of nanodiamond to form a gap-plasmon waveguide. Adapted with permission.[42] Copyright 2018, The American Chemical society.

be obtained together with efficient channeling of photons from single photon emitters into these waveguide modes. In an experiment, a gap-plasmon waveguide mode was excited by a single NV center.[42] **Figure 6**a shows a schematic of the experiment. Single NV center contained in a nanodiamond was put in the gap between nanowire-flake air gap. The NV center, excited by the green laser, emits in the gap-plasmon waveguide mode. Single plasmons generated in the gap mode propagates to waveguide mode and get scattered to far-field. In Figure 6b, simulations results obtained for an optimally oriented emitter emitting at a wavelength of 700 nm, is shown. Dimensions corresponding to the system presented in this section, that is, wire diameter 210 nm and gap 16nm was used in the simulations. In Figure 6c, β-factor vs position is plotted, where one can observe that the β-factor can be up to 0.97, for this system.

In this experiment, HSQ pads of dimensions 5 μm × 5 μm and 1 μm separation with a thickness of ≈20 nm were created on silver flakes, using e-beam lithography. Nanodiamonds containing NV-centers, followed by silver nanowires were spin-coated on the sample. Nanodiamonds containing single NV centers were determined in a similar way as described in Section 3.2. An AFM cantilever tip was then utilized to move the nanodiamond in-between HSQ pads. Subsequently, a silver nanowire, which was found close to the nanodiamond, was moved on top to complete the assembly of the coupled system. In Figure 6d, an AFM image of such a system is shown. The NV center in the coupled system was excited continuously with a CW laser at 532 nm wavelength, and a fluorescence image was captured with a camera. In the image, shown in Figure 6e, there are three spots. There is emission from the NV center into the far-field, in-addition there are two more emission spots corresponding to ends of the silver nanowire. The decay-rate of the NV center was enhanced because the NV-center got coupled to the confined mode. In Figure 6f, the NV center lifetimes before and after assembly of the coupled system are presented. The emission-rate was estimated to be ≈14.7 times enhanced. NV centers in nanodiamonds on a silver surface have enhanced decay-rate, on average, compared to when they are placed on glass, as mentioned in Section 3.2. The total decay-rate, for this structure, is enhanced by a factor of ≈29.4. By repeating this experiment seven times, decay-rate enhancements up to ≈50, and FOM up to ≈212 were obtained.

Although, high FOM can be obtained for such systems, fabricating a complicated structure with the method utilized in this experiment will be challenging. Therefore, another fabrication method need to be used for making use of these gap-plasmon waveguides in a scalable system. In this direction, gap-plasmon waveguides have been fabricated using focussed ion beam milling of mono-crystalline silver flakes and coupled to quantum emitters.[68–72]

3.4. Coupling Single Emitters to Hybrid Plasmonic Waveguide

When a metal surface is coated with a thin layer of low-index material and a high-index nanowire is put on top, the structure formed supports a hybrid plasmonic mode. Such modes are highly confined and at the same time the propagation lengths are longer,[73,74] compared to gap-plasmon modes for example. Therefore, such a waveguide mode will allow for high FOM in a

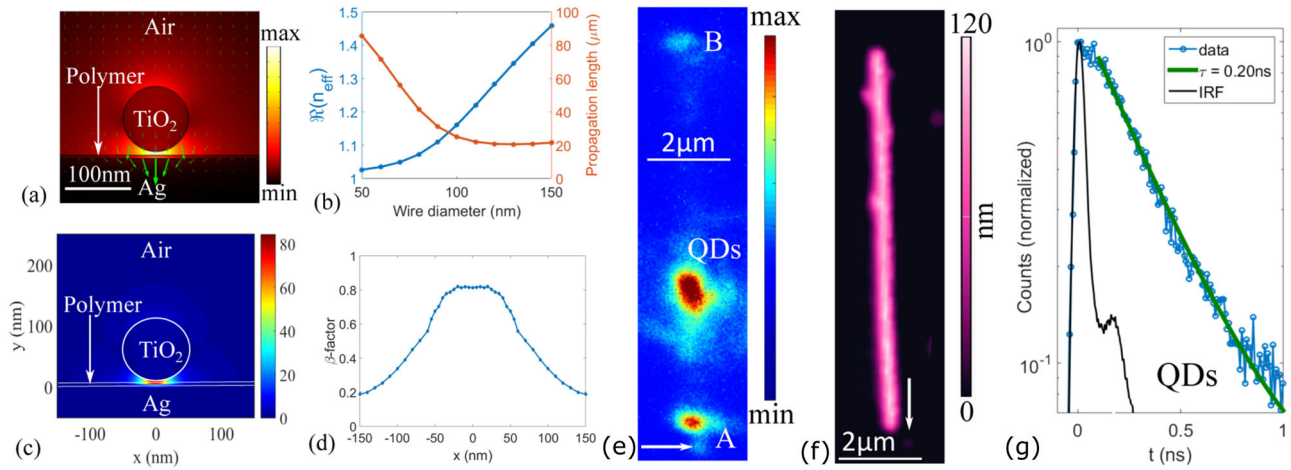

Figure 7. a) Normalized electric field plotted as a function of position, with arrows indicating the direction of electric field at its tail. b) Real part of effective mode index and propagation lengths vs diameter of titanium oxide nanowire. c) Decay-rate of emitter into the hybrid plasmonic mode, normalized to its decay-rate in vacuum. d) β-factor vs x-position, for a fixed y= 8 nm. e) Fluorescence image captured, while QDs spot was continuously excited. f) AFM image of the titanium oxide nanowire and QDs on top of silver flake forming a coupled system. g) Measured data and a tail fit with single exponential, for the spot QDs in (e). The figure also shows the instrument response function (IRF). Adapted with permission.[43] Copyright 2019, The American Chemical Society.

coupled system. In ref. [43], such a waveguide is coupled to colloidal quantum dots. In the experiment, colloidal quantum dots emitting at 630nm with mean diameter of 6 nm were used. Hybrid plasmonic waveguide structure was obtained by first coating monocrystalline silver flakes by a polymer, followed by spin-coating QDs and titanium oxide nanowires. The polymer thickness used was 5 nm and the mean diameter of titanium oxide nanowires used was 100 nm.

The structure formed was simulated with FEM using a commercial software (COMSOL Multiphysics). The waveguide modes were calculated while varying the titanium oxide nanowire diameter around 100nm. An air gap of 6nm between polymer (corresponding to QD diameter) and the nanowire was assumed. Refractive indices of 2.4 and 1.5 for titanium oxide and the polymer, respectively, was used. In **Figure 7**a, the electric field distribution for the mode is shown, for the nanowire diameter of 100nm. The real part of the effective mode index and propagation lengths as a function of nanowire diameter, are shown in Figure 7b. Decay-rate into the hybrid mode, normalized by its decay-rate in vacuum, is shown in Figure 7c. The emitter orientation is assumed to be along the electric-field, and therefore, the plotted decay-rates are maximum possible decay-rates at any given position. The β-factor can be up to 0.83, as can be seen in the plot of β-factor vs the x-position, y-position fixed at 8 nm, in Figure 7d. Simulation results suggest that hybrid plasmonic mode supported by the structure is promising for coupling to an emitter, as the decay-rate and β-factor can be high in combination with long propagation lengths.

In Figure 7e, we present fluorescence image of a QD coupled to the hybrid mode, supported by titanium oxide nanowire and silver flake with a low-index gap. It can be observed that there are two more spots A and B other than QDs, which clearly suggest that QDs emit into the waveguide. The emission propagates to the waveguide ends, and subsequently gets scattered to the far-field. Figure 7f shows an AFM image of the coupled system, formed by titanium oxide nanowire, QDs and the polymer coated silver flake. In Figure 7g, the decay-curve and instrument response function (IRF) are shown. The lifetime of the QDs coupled to the waveguide is ≈0.2 ns. The average lifetime of QDs on a glass substrate, in this experiment, was found to be ≈8.3 ns. Therefore, the decay-rate enhancement on average is ≈41.5. The propagation length and β-factor estimated experimentally are 7.5 μm and 0.73, respectively. Therefore, the FOM obtained is 361. This is the highest FOM obtained for experimentally demonstrated quantum emitter–plasmonic waveguide coupled system. For this system, another fabrication method is needed to make it scalable.

We have discussed four different plasmonic waveguides in this section. Wedge waveguides provides a balance with high confinement and long propagation length, but to make more complicated circuitry with such waveguides will be difficult while maintaining the high quality of wedge waveguides. It is also challenging to put the SPEs near the tip of the wedge waveguides. DLSPP waveguides offer a flexible platform for fabrication of waveguide circuits where SPEs can be embedded inside the waveguides. However, the DLSPP waveguide mode cannot be very confined and therefore high decay-rate enhancements cannot be obtained. Although, recently, enlargement of decay-rate enhancement by a DLSPP waveguide by inserting a dielectric layer has been demonstrated,[75] there is a limit to the confinement of such waveguides. Gap-plasmon waveguides can support very confined mode, and in principle, waveguide circuitry can be fabricated utilizing a similar technique as in the case of DLSPPW. However, the propagation losses are high even when monocrystalline silver is used. So, with lithographically made polycrystalline metallic wires, losses will be higher and because of the structure the confinement will be lower. Hybrid plasmonic waveguide modes can provide a combination where a high decay-rate enhancement can be combined with long propagation distances, therefore a high FOM was obtained experimentally for such structures. Lithographic methods can be used for obtaining such structures, but the propagation loss and confinement will

be lower due to weaker confinement and polycrystalline nature of the high index dielectric.

Above experiments were demonstrations where high confinement was utilized for the channeling of emission and decay-rate enhancement of the quantum emitter. Some structures can be utilized for further enhancement and more efficient channeling of emission into plasmonic waveguides. In the next section, we present two such structures that have been utilized for enhanced emission rate as well as channeling into DLSPP waveguides, and can be used for any waveguide, in principle.

4. Bragg Cavities and Mirrors for Efficient Channeling of Emission into Plasmonic Waveguides

NV center in diamonds have a broad spectral width at room temperature. With a plasmonic waveguide, entire spectrum of an NV center can be enhanced. Whereas, with a Bragg plasmonic cavity, certain parts of the emission spectrum of NV-center can be enhanced. This can result in a narrow-band single-photon source, with a possibility to choose the emission wavelength.[76] In this configuration, the waveguide structure is combined with a Bragg cavity to enhance and channel emission that is in resonance with the cavity. With e-beam lithography, by fabrication of HSQ structure around a single NV-center contained in a nanodiamond using a technique that is described in Section 3.2, one can obtain DLSPP waveguides in combination with two distributed Bragg reflectors (DBRs) forming a cavity.

In **Figure 8**a, an SEM image of such a cavity is presented. A fluorescence image is shown in Figure 8b, where the NV center positioned inside the cavity is continuously excited. The emission is enhanced at the cavity resonance, and the emission from waveguide ends can be observed to be filtered in a narrow-band spectrum. In Figure 8c, the enhanced region of NV center emission spectrum obtained from a cavity is compared with a reference DLSPP waveguide. By comparing the two spectra, a sixfold enhancement by the cavity, at zero phonon line (ZPL), was estimated. Considering the emission enhancement by the DLSPP waveguide, in addition enhancement by the cavity, the total decay-rate enhancement (Γ_{tot}/Γ_0), was estimated to be 42 at ZPL.

In the following, we describe another useful configuration, a distributed Bragg mirror, that was utilized for unidirectional coupling of emission in a DLSPP waveguide.[77] A GeV center was used for this demonstration. Furthermore, cryogenic temperature was used to obtain a narrow band emission. In this experiment, colloidal gold crystal flakes were used as plasmonic material. Gold flakes were made following the recipe from ref. [78]. Alignment markers were made on the gold crystals, and subsequently NDs were deposited on the substrate following the process described in Section 3.2. Optical measurements were performed at 4.7K in the cold finger of a continuous-flow helium cryostat. Single GeV centers were found based on measurements of their properties. By utilizing techniques as described in Section 3.2, a waveguide-mirror combination with Bragg gratings (BGs) were fabricated to incorporate the ND in the waveguide. NDs were placed at constructive interference point, that is, at $d = 3\lambda_n/4$, λ_n being the plasmonic mode's effective wavelength,[79] as shown in **Figure 9**a. With such positioning, the decay-rate can be

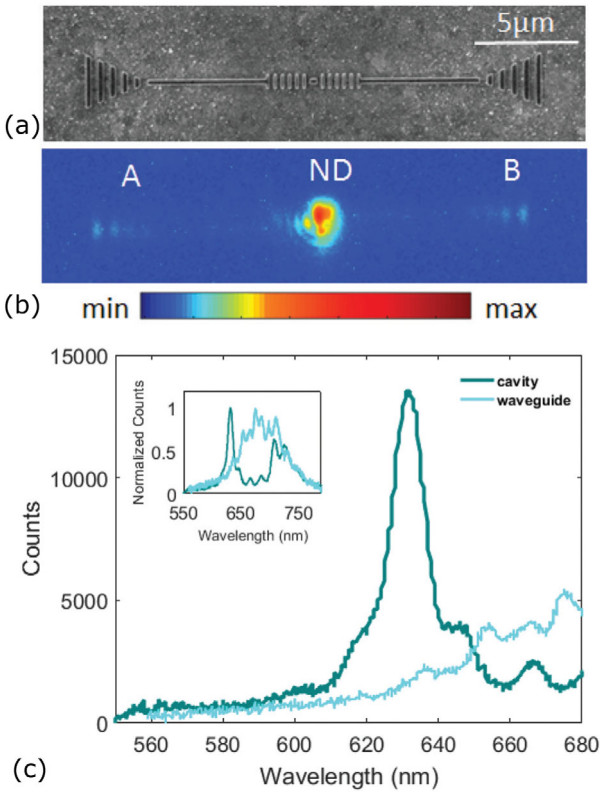

Figure 8. a) SEM image of cavity and waveguide, fabricated to contain a single NV center. b) Fluorescence image of the structure, with the NV center excited by 532 nm CW laser. c) Comparison of emission spectra when an NV center is coupled to a DLSPP waveguide and that to a cavity resonant at ZPL of NV center. The inset shows entire NV center emission spectrum coupled to a DLSPP waveguide (cyan), and that coupled to a cavity (dark green), respectively. Adapted with permission.[76] Copyright 2017, The Royal Society of Chemistry.

enhanced by a factor of $(1 + R)^2$, R being the reflectance of the BG mirror.

An SEM image of the structure fabricated on top of a gold flake is shown in Figure 9b. The fluorescence image shown in Figure 9c, was captured while exciting the GeV-ND with a 532 nm laser. The image has two spots, corresponding to GeV-ND and to the out-coupler end. Emission from the out-coupler end suggests emission of GeV center into the DLSPP waveguide mode. Fluorescence spectra measured at the GeV-ND spot and that from the out-coupling grating are shown in Figure 9d and e, respectively. A shift in ZPL from 602 to 605 nm was observed. This can happen due to an isotopic substitution of the germanium atom.[80] Lifetime measurements before and after structure fabrication indicated a five times decay-rate enhancement, lifetime changed from 11.2 ns before structure fabrication to 2.3 ns for the GeV-ND incorporated in the device. With an additional two times lifetime reduction due to the metal layer taken into consideration,[41] the total decay-rate enhancement by a factor of ten was reported for GeV center in this coupled system.

The two configurations presented above can be utilized for any waveguide, in principle. This way coupling of emission to plasmonic waveguides can be further enhanced and total emission can be channeled more efficiently.

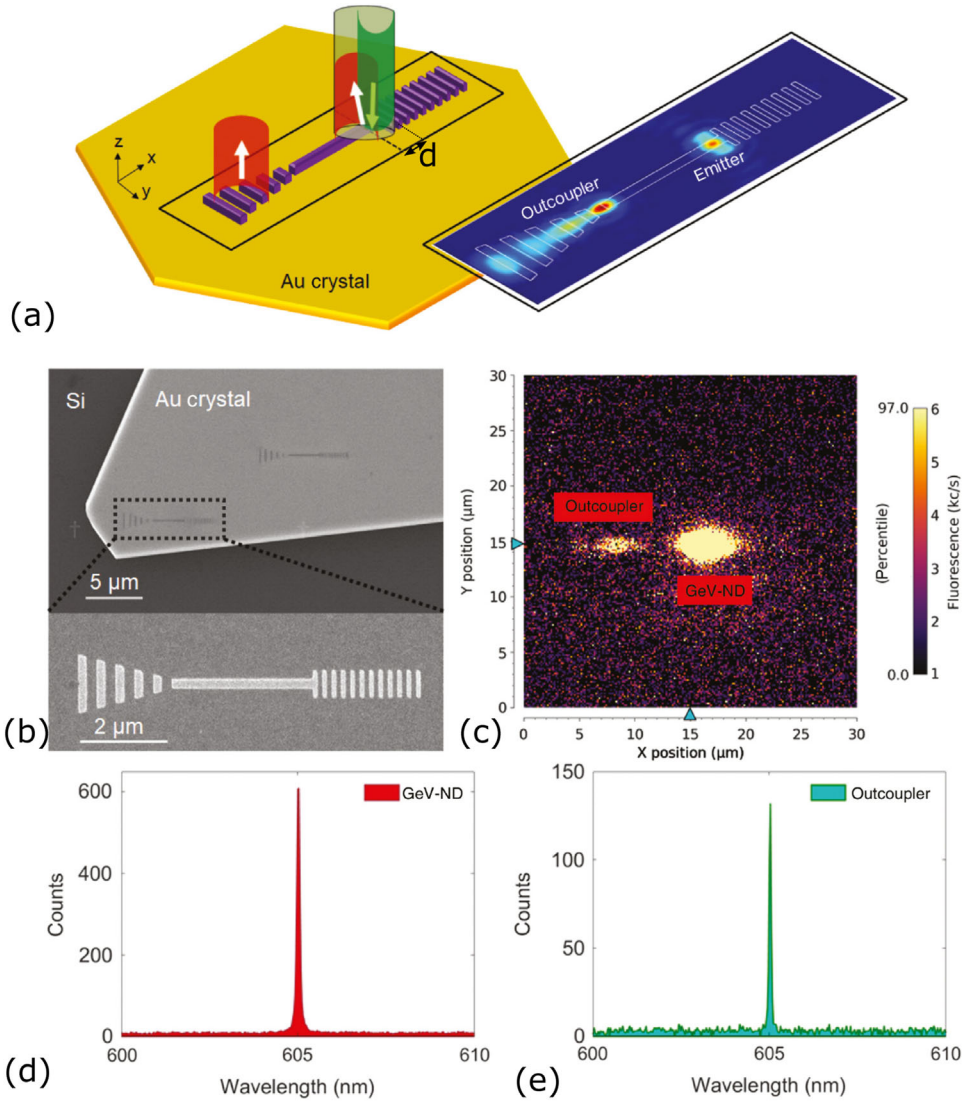

Figure 9. a) Schematic showing the working principle in this experiment. Bragg grating formed by dielectric ridges were fabricated on top of gold flakes along with a DLSPP waveguide, and the GeV center was positioned at a distance d from the BG mirror. b) SEM image of the device, having a grating period of 240nm. c) Fluorescence image of the coupled system, while the GeV center is excited. d) Spectrum measured at the GeV-ND spot. e) spectrum measured at the end B. Adapted with permission.[77] Copyright 2020, The Authors, published by De Gruyter.

5. Enhanced Non-Linearity at Single Quantum Emitter Level

Confinement of plasmonic modes benefits the non-linear effects as well. Stimulated emission is one example which depends super-linearly on the intensity of light. In ref. [72], nonlinearity at single molecule level has been demonstrated. A gap-plasmonic waveguide structure has been utilized for this demonstration. In **Figure 10**a, the mode confinement of the plasmonic waveguide is compared to a diffraction-limited Gaussian focus with numerical aperture (NA) of 1.4. A 50× intensity in the plasmonic waveguide can be observed by comparing the two panels of Figure 10a.

The scheme utilized for observing the stimulated emission is similar to what is utilized for stimulated emission depletion (STED) microscopy. Here, we briefly describe the scheme. Using a pump pulse, the terrylene diimide (TDI) molecule can be excited from its ground state to its vibrational sideband of the electronic excited state. The molecule relaxes very fast, within a few ps, to the vibrational ground state of the electronic excited state. A second laser pulse can then be used, with appropriately chosen wavelength to get stimulated emission into a high vibrational band of the ground electronic state. After shining the second pulse, the fluorescence emission in the wavelength range in-between the two laser pulses, is checked. Stimulated emission is indicated by a decrease in the fluorescence from the molecule. This scheme is illustrated in Figure 10b.

By spin-coating a low concentration of TDI molecules, single TDI molecules could be found in the gap of the waveguide. By shining the excitation laser pulse on the antenna with a polarization perpendicular to the waveguide, anti-symmetric mode was

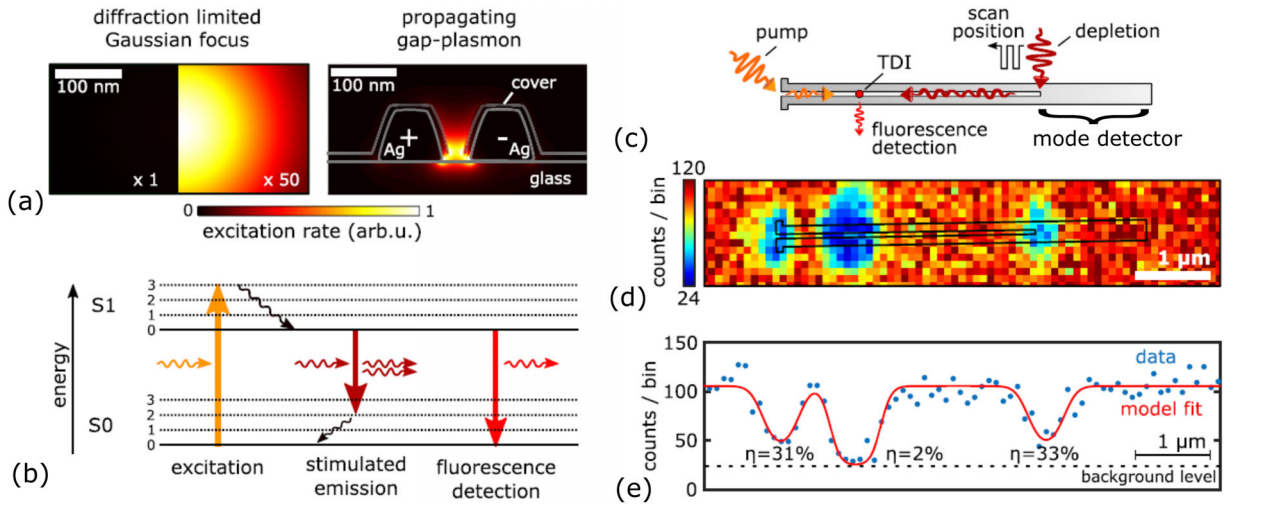

Figure 10. a) Comparison of a diffraction limited Gaussian focus (NA 1.4) and the gap-mode of a plasmonic slot waveguide. b) Scheme utilized for detection of stimulated emission. After the excitation of molecule and its relaxation to vibrational ground state of electronic excited state, a second laser pulse is utilized to cause stimulated emission. The probability of the excited state to undergo stimulated emission is monitored by fluorescence counts. c) The molecule excited by focusing a pump pulse on the antenna, while the depletion pulse is raster scanned over the sample. The detected fluorescence is a measure of the stimulated emission the molecule undergoes. d) Fluorescence map recoreded while the depletion laser was scanned. e) The data profile and a model fit along a line close to the center of the slot waveguide. Adapted with permission.[72] Copyright 2020, The American Chemical Society.

excited. This laser pulse coupled into the waveguide then excites the TDI molecule. After 50ps of shining the excitation laser the depletion laser is shined. The depletion laser is scanned over the waveguide structure while the excitation laser is kept on the antenna. While scanning the depletion laser, the molecule fluorescence is measured directly in the far-field. A schematics of the scanning process is shown in Figure 10c.

The fluorescence lifetime changed from 3.6 ns for molecules not coupled to waveguides, to 0.4 ns for the molecules found in the gap of the waveguide, that is, lifetime reduced by around one order of magnitude. In the fluorescence intensity map, presented in Figure 10d, one can observe that fluorescence is maximum whenever the depletion pulse does not reach the molecule. With the depletion pulse focused on the molecule, stimulated emission happens and therefore fluorescence emission is suppressed. The same effect could be observed when the depletion pulse is focused on the antenna or the inner end of the mode detector. A fluorescence suppression larger than 30% of the maximum value was observed, as shown in Figure 10e. When the depletion pulse was focused on antenna of the inner end of the mode detector, it excited antisymmetric waveguide mode which propagated to the molecule and caused stimulated emission. Therefore, a single TDI molecule was demonstrated to undergo the stimulated emission by plasmons.

6. Conclusion

We have provided an overview of various plasmonic waveguide coupled with single photon emitter. Quantum emitter–plasmonic waveguide systems with high FOM have great potential to be used in a quantum optical network, which can be highly compact. A few applications have been demonstrated such as non-linearity at single molecule level and read-out of electronic spins for NV centers coupled to plasmonic waveguides.[72,81] Recent proposals of nanoantenna based enhancement of emission rate and channeling of emission into plasmonic waveguides will increase the FOM by orders of magnitude.[82,83] Boosting up the emission enhancement with properly engineered nanostructured environment suggests a fascinating prospect of realizing room-temperature generation of indistinguishable photons.[21] Apart from enhancing the decay-rates of emitters, plasmonic waveguides can also be utilized for engineering emission pattern and polarization of single photon emitters.[84] Furthermore, on-chip detection of plasmons and plasmon-plasmon quantum interference have also been demonstrated.[85–87] The main challenge in using plasmonic waveguides for quantum optical on-chip circuits is propagation loss in the waveguides. Therefore, utilizing plasmonic waveguides as antennas for the emitters to couple into dielectric waveguides and using dielectric waveguides for the circuitry is required, that is, with a hybrid approach one can take advantage of plasmonic as well as dielectric waveguides. In the near future, it should be possible to demonstrate the generation of single plasmons, quantum circuitry and detection of plasmons on the same chip by propitiously making use of integration with nanophotonic (low-loss) waveguides. This will pave the way to realizing very compact and efficient quantum optical on-chip circuits.

Acknowledgements

The authors acknowledge financial support from VILLUM FONDEN by a research grant (35950) and Villum Kann Rasmussen Foundation (Award in Technical and Natural Sciences 2019).

Conflict of Interest

The authors declare no conflict of interest.

Keywords

plasmonic waveguide, single photons, single plasmons, quantum emitter, quantum plasmonics

Received: April 8, 2021
Revised: July 20, 2021
Published online:

[1] E. Knill, R. Laflamme, G. Milburn, *Nature* **2001**, *409*, 46.
[2] J. L. O'Brien, *Science* **2007**, *318*, 1567.
[3] H. J. Kimble, *Nature* **2008**, *453*, 1023.
[4] S. Slussarenko, G. J. Pryde, *Appl. Phys. Rev.* **2019**, *6*, 041303.
[5] D. B. Higginbottom, L. Slodicka, G. Araneda, L. Lachman, R. Filip, M. Hennrich, R. Blatt, *New J. Phys.* **2016**, *18*, 093038.
[6] I. Aharonovich, D. Englund, M. Toth, *Nat. Photonics* **2016**, *10*, 631.
[7] Y. Arakawa, M. J. Holmes, *Appl. Phys. Rev.* **2020**, *7*, 021309.
[8] C. Jennings, X. Ma, T. Wickramasinghe, M. Doty, M. Scheibner, E. Stinaff, M. Ware, *Adv. Quantum Technol.* **2020**, *3*, 1900085.
[9] G. Zhang, Y. Cheng, J.-P. Chou, A. Gali, *Appl. Phys. Rev.* **2020**, *7*, 031308.
[10] X. Liu, M. C. Hersam, *Nat. Rev. Mater.* **2019**, *4*, 669.
[11] S. Rodt, S. Reitzenstein, T. Heindel, *J. Phys.: Condens. Matter* **2020**, *32*, 153003.
[12] X. Cao, M. Zopf, F. Ding, *J. Semicond.* **2019**, *40*, 071901.
[13] P. P. J. Schrinner, J. Olthaus, D. E. Reiter, C. Schuck, *Nano Lett.* **2020**, *20*, 8170.
[14] X.-L. Chu, T. Pregnolato, R. Schott, A. D. Wieck, A. Ludwig, N. Rotenberg, P. Lodahl, *Adv. Quantum Technol.* **2020**, *3*, 2000026.
[15] P. Tuerschmann, H. Le Jeannic, S. F. Simonsen, H. R. Haakh, S. Goetzinger, V. Sandoghdar, P. Lodahl, N. Rotenberg, *Nanophotonics* **2019**, *8*, 1641.
[16] S. I. Bozhevolnyi, J. B. Khurgin, *Optica* **2016**, *3*, 1418.
[17] S. Bozhevolnyi, J. Khurgin, *Nat. Photonics* **2017**, *11*, 398.
[18] A. Kinkhabwala, Z. Yu, S. Fan, Y. Avlasevich, K. Muellen, W. E. Moerner, *Nat. Photonics* **2009**, *3*, 654.
[19] G. M. Akselrod, C. Argyropoulos, T. B. Hoang, C. Ciracì, C. Fang, J. Huang, D. R. Smith, M. H. Mikkelsen, *Nat. Photonics* **2014**, *8*, 835.
[20] T. B. Hoang, G. M. Akselrod, M. H. Mikkelsen, *Nano Lett.* **2016**, *16*, 270.
[21] S. I. Bogdanov, O. A. Makarova, X. Xu, Z. O. Martin, A. S. Lagutchev, M. Olinde, D. Shah, S. N. Chowdhury, A. R. Gabidullin, I. A. Ryzhikov, I. A. Rodionov, A. V. Kildishev, S. I. Bozhevolnyi, A. Boltasseva, V. M. Shalaev, J. B. Khurgin, *Optica* **2020**, *7*, 463.
[22] A. I. Fernández-Domínguez, S. I. Bozhevolnyi, N. A. Mortensen, *ACS Photonics* **2018**, *5*, 3447.
[23] D. E. Chang, A. S. Sørensen, P. R. Hemmer, M. D. Lukin, *Phys. Rev. Lett.* **2006**, *97*, 053002.
[24] Y. Chen, T. R. Nielsen, N. Gregersen, P. Lodahl, J. Mørk, *Phys. Rev. B* **2010**, *81*, 125431.
[25] J.-T. Shen, S. Fan, *Phys. Rev. Lett.* **2007**, *98*, 153003.
[26] D. E. Chang, A. S. Sørensen, E. A. Demler, M. D. Lukin, *Nat. Phys.* **2007**, *3*, 807.
[27] L. Zhou, Z. R. Gong, Y.-x. Liu, C. P. Sun, F. Nori, *Phys. Rev. Lett.* **2008**, *101*, 100501.
[28] D. Martín-Cano, L. Martín-Moreno, F. J. García-Vidal, E. Moreno, *Nano Lett.* **2010**, *10*, 3129.
[29] D. Roy, *Phys. Rev. Lett.* **2011**, *106*, 053601.
[30] H. Zheng, D. J. Gauthier, H. U. Baranger, *Phys. Rev. Lett.* **2013**, *111*, 090502.
[31] H. Zheng, H. U. Baranger, *Phys. Rev. Lett.* **2013**, *110*, 113601.
[32] Y.-L. L. Fang, H. Zheng, H. U. Baranger, *EPJ Quantum Technol.* **2014**, *1*, 3.
[33] D. Gramotnev, S. Bozhevolnyi, *Nat. Photonics* **2010**, *4*, 83.
[34] Z. Han, S. I. Bozhevolnyi, *Rep. Prog. Phys.* **2012**, *76*, 016402.
[35] W. L. Barnes, S. A. R. Horsley, W. L. Vos, *J. Opt.* **2020**, *22*, 073501.
[36] A. V. Akimov, A. Mukherjee, C. L. Yu, D. E. Chang, A. S. Zibrov, P. R. Hemmer, H. Park, M. D. Lukin, *Nature* **2007**, *450*, 402.
[37] S. Kumar, A. Huck, U. L. Andersen, *Nano Lett.* **2013**, *13*, 1221.
[38] E. Bermúdez-Ureña, C. Gonzalez-Ballestero, M. Geiselmann, R. Marty, I. P. Radko, T. Holmgaard, Y. Alaverdyan, E. Moreno, F. J. Garcia-Vidal, S. I. Bozhevolnyi, R. Quidant, *Nat. Commun.* **2015**, *6*, 7883.
[39] S. J. P. Kress, F. V. Antolinez, P. Richner, S. V. Jayanti, D. K. Kim, F. Prins, A. Riedinger, M. P. C. Fischer, S. Meyer, K. M. McPeak, D. Poulikakos, D. J. Norris, *Nano Lett.* **2015**, *15*, 6267.
[40] H. Siampour, S. Kumar, S. I. Bozhevolnyi, *ACS Photonics* **2017**, *4*, 1879.
[41] H. Siampour, S. Kumar, V. A. Davydov, L. F. Kulikova, V. N. Agafonov, S. I. Bozhevolnyi, *Light: Sci. Appl.* **2018**, *7*, 61.
[42] S. Kumar, S. K. Andersen, S. I. Bozhevolnyi, *ACS Photonics* **2019**, *6*, 23.
[43] S. Kumar, S. I. Bozhevolnyi, *ACS Photonics* **2019**, *6*, 1587.
[44] R. Kolesov, B. Grotz, G. Balasubramanian, R. J. Stöhr, A. A. L. Nicolet, P. R. Hemmer, F. Jelezko, J. Wrachtrup, *Nat. Phys.* **2009**, *5*, 470.
[45] A. Huck, S. Kumar, A. Shakoor, U. L. Andersen, *Phys. Rev. Lett.* **2011**, *106*, 096801.
[46] S. Kumar, A. Huck, Y.-W. Lu, U. L. Andersen, *Opt. Lett.* **2013**, *38*, 3838.
[47] S. Kumar, A. Huck, Y. Chen, U. L. Andersen, *Appl. Phys. Lett.* **2013**, *102*, 103106.
[48] C. Gruber, A. Trügler, A. Hohenau, U. Hohenester, J. R. Krenn, *Nano Lett.* **2013**, *13*, 4257.
[49] S. Kumar, N. I. Kristiansen, A. Huck, U. L. Andersen, *Nano Lett.* **2014**, *14*, 663.
[50] Q. Li, H. Wei, H. Xu, *Nano Lett.* **2015**, *15*, 8181.
[51] S. Kumar, V. A. Davydov, V. N. Agafonov, S. I. Bozhevolnyi, *Opt. Mater. Express* **2017**, *7*, 2586.
[52] K.-Y. Jeong, S. W. Lee, J.-H. Choi, J.-P. So, H.-G. Park, *Nanomaterials* **2020**, *10*, 1663.
[53] S. Kumar, T. Leißner, S. Boroviks, S. K. H. Andersen, J. Fiutowski, H.-G. Rubahn, N. A. Mortensen, S. I. Bozhevolnyi, *ACS Photonics* **2020**, *7*, 2211.
[54] A. Huck, U. L. Andersen, *Nanophotonics* **2016**, *5*, 483.
[55] S. Grandi, M. P. Nielsen, J. Cambiasso, S. Boissier, K. D. Major, C. Reardon, T. F. Krauss, R. F. Oulton, E. A. Hinds, A. S. Clark, *APL Photonics* **2019**, *4*, 086101.
[56] D. E. Westmoreland, K. P. McClelland, K. A. Perez, J. C. Schwabacher, Z. Zhang, E. A. Weiss, *J. Chem. Phys.* **2019**, *151*, 210901.
[57] M. W. Doherty, N. B. Manson, P. Delaney, F. Jelezko, J. Wrachtrup, L. C. Hollenberg, *Phys. Rep.* **2013**, *528*, 1.
[58] A. Sipahigil, M. L. Goldman, E. Togan, Y. Chu, M. Markham, D. J. Twitchen, A. S. Zibrov, A. Kubanek, M. D. Lukin, *Phys. Rev. Lett.* **2012**, *108*, 143601.
[59] H. Bernien, L. Childress, L. Robledo, M. Markham, D. Twitchen, R. Hanson, *Phys. Rev. Lett.* **2012**, *108*, 043604.
[60] E. Togan, Y. Chu, A. S. Trifonov, L. Jiang, J. Maze, L. Childress, M. V. G. Dutt, A. S. Sørensen, P. R. Hemmer, A. S. Zibrov, M. D. Lukin, *Nature* **2010**, *466*, 730.
[61] H. Bernien, B. Hensen, W. Pfaff, G. Koolstra, M. S. Blok, L. Robledo, T. H. Taminiau, M. Markham, D. J. Twitchen, L. Childress, R. Hanson, *Nature* **2013**, *497*, 86.
[62] W. Pfaff, B. J. Hensen, H. Bernien, S. B. van Dam, M. S. Blok, T. H. Taminiau, M. J. Tiggelman, R. N. Schouten, M. Markham, D. J. Twitchen, R. Hanson, *Science* **2014**, *345*, 532.
[63] B. Hensen, H. Bernien, A. E. Dreaú, A. Reiserer, N. Kalb, M. S. Blok, J. Ruitenberg, R. F. L. Vermeulen, R. N. Schouten, C. Abellán, W. Amaya,

V. Pruneri, M. W. Mitchell, M. Markham, D. J. Twitchen, D. Elkouss, S. Wehner, T. H. Taminiau, R. Hanson, *Nature* **2015**, *526*, 682.
[64] P. C. Humphreys, N. Kalb, J. P. J. Morits, R. N. Schouten, R. F. L. Vermeulen, D. J. Twitchen, M. Markham, R. Hanson, *Nature* **2018**, *558*, 268.
[65] C. Kurtsiefer, S. Mayer, P. Zarda, H. Weinfurter, *Phys. Rev. Lett.* **2000**, *85*, 290.
[66] T. Iwasaki, F. Ishibashi, Y. Miyamoto, Y. Doi, S. Kobayashi, T. Miyazaki, K. Tahara, K. D. Jahnke, L. J. Rogers, B. Naydenov, F. Jelezko, S. Yamasaki, S. Nagamachi, T. Inubushi, N. Mizuochi, M. Hatano, *Sci. Rep.* **2015**, *5*, 12882.
[67] M. K. Bhaskar, D. D. Sukachev, A. Sipahigil, R. E. Evans, M. J. Burek, C. T. Nguyen, L. J. Rogers, P. Siyushev, M. H. Metsch, H. Park, F. Jelezko, M. Lončar, M. D. Lukin, *Phys. Rev. Lett.* **2017**, *118*, 223603.
[68] S. Kumar, Y.-W. Lu, A. Huck, U. L. Andersen, *Opt. Express* **2012**, *20*, 24614.
[69] M. Blauth, M. Jürgensen, G. Vest, O. Hartwig, M. Prechtl, J. Cerne, J. J. Finley, M. Kaniber, *Nano Lett.* **2018**, *18*, 6812.
[70] C. Schörner, S. Adhikari, M. Lippitz, *Nano Lett.* **2019**, *19*, 3238.
[71] S. Grandi, M. P. Nielsen, J. Cambiasso, S. Boissier, K. D. Major, C. Reardon, T. F. Krauss, R. F. Oulton, E. A. Hinds, A. S. Clark, *APL Photonics* **2019**, *4*, 086101.
[72] C. Schörner, M. Lippitz, *Nano Lett.* **2020**, *20*, 2152.
[73] R. Oulton, V. Sorger, D. Genov, D. Pile, X. Zhang, *Nat. Photonics* **2008**, *2*, 496.
[74] I. Avrutsky, R. Soref, W. Buchwald, *Opt. Express* **2010**, *18*, 348.
[75] G. Zhang, H. Liu, S. Jia, H. Li, Z. Li, Q. Gong, J. Chen, *Adv. Quantum Technol.* **2020**, *3*, 2000033.
[76] H. Siampour, S. Kumar, S. I. Bozhevolnyi, *Nanoscale* **2017**, *9*, 17902.
[77] H. Siampour, O. Wang, V. A. Zenin, S. Boroviks, P. Siyushev, Y. Yang, V. A. Davydov, L. F. Kulikova, V. N. Agafonov, A. Kubanek, N. A. Mortensen, F. Jelezko, S. I. Bozhevolnyi, *Nanophotonics* **2020**, *9*, 953.
[78] S. Boroviks, C. Wolff, J. Linnet, Y. Yang, F. Todisco, A. S. Roberts, S. I. Bozhevolnyi, B. Hecht, N. A. Mortensen, *Opt. Mater. Express* **2018**, *8*, 3688.
[79] F. Lopez-Tejeira, S. Rodrigo, L. Martin-Moreno, F. Garcia-Vidal, E. Devaux, T. Ebbesen, J. Krenn, I. Radko, S. Bozhevolnyi, M. Gonzalez, J.-C. Weeber, A. Dereux, *Nat. Phys.* **2007**, *3*, 324.
[80] E. A. Ekimov, V. S. Krivobok, S. G. Lyapin, P. S. Sherin, V. A. Gavva, M. V. Kondrin, *Phys. Rev. B* **2017**, *95*, 094113.
[81] Z. Al-Baiaty, B. P. Cumming, X. Gan, M. Gu, *Nanoscale Adv.* **2019**, *1*, 3131.
[82] G. Zhang, S. Jia, Y. Gu, J. Chen, *Laser Photonics Rev.* **2019**, *13*, 1900025.
[83] Y. Ma, J. Li, M. Cada, Y. Bian, Z. Han, Y. Ma, M. Iqbal, J. Pištora, *IEEE J. Sel. Top. Quantum Electron.* **2021**, *27*, 4600307.
[84] G. Zhang, Y. Gu, Q. Gong, J. Chen, *Nanophotonics* **2020**, *9*, 3557.
[85] R. W. Heeres, S. N. Dorenbos, B. Koene, G. S. Solomon, L. P. Kouwenhoven, V. Zwiller, *Nano Lett.* **2010**, *10*, 661.
[86] R. Heeres, L. Kouwenhoven, V. Zwiller, *Nat. Nanotechnol.* **2013**, *8*, 719.
[87] Y.-J. Cai, M. Li, X.-F. Ren, C.-L. Zou, X. Xiong, H.-L. Lei, B.-H. Liu, G.-P. Guo, G.-C. Guo, *Phys. Rev. Applied* **2014**, *2*, 014004.

Shailesh Kumar is an assistant professor at the Centre for Nano Optics at University of Southern Denmark. He obtained his Ph.D. degree in Physics from Technical University of Denmark, Denmark in 2012. His area of research includes light–matter interaction, quantum plasmonics, and integrated quantum optics.

Sergey I. Bozhevolnyi is a professor and centre leader of the Centre for Nano Optics at University of Southern Denmark. He obtained his Ph.D. degree in Physics from Moscow Institute of Physics and Technology, Russia in 1981. His research areas include quantum plasmonics, light–matter interaction, and active meta-surfaces.